Low-temperature magnetoresistance of (111) $(La_{0.3}Sr_{0.7})(Al_{0.65}Ta_{0.35})O_3/SrTiO_3$

V. V. Bal,[1] Z. Huang,[2,3] K. Han,[2,3] Ariando,[2,3] T. Venkatesan,[2,3,4,5,6] and V. Chandrasekhar[1,*]
[1]*Department of Physics and Astronomy, Northwestern University, Evanston, Illinois 60208, USA*
[2]*NUSNNI-Nanocore, National University of Singapore, 117411 Singapore*
[3]*Department of Physics, National University of Singapore, 117551 Singapore*
[4]*NUS Graduate School for Integrative Sciences and Engineering, National University of Singapore, 117456 Singapore*
[5]*Department of Electrical and Computer Engineering, National University of Singapore, 117576 Singapore*
[6]*Department of Material Science and Engineering, National University of Singapore, 117575 Singapore*

(Received 2 March 2018; revised manuscript received 16 November 2018; published 3 January 2019)

The two-dimensional conducting interfaces in $SrTiO_3$-based systems are known to show a variety of coexisting and competing phenomena in a complex phase space. Magnetoresistance measurements, which are typically used to extract information about the various interactions in these systems, must be interpreted with care, since multiple interactions can contribute to the resistivity in a given range of magnetic field and temperature. Here we review all the phenomena that can contribute to transport in $SrTiO_3$-based conducting interfaces at low temperatures. We apply this understanding to the perpendicular magnetoresistance data of the high-mobility system of (111) oriented $(La_{0.3}Sr_{0.7})(Al_{0.65}Ta_{0.35})O_3$/STO heterostructures, and find an excess negative magnetoresistance contribution which cannot be explained by weak localization alone. We argue that contributions from magnetic scattering as well as electron-electron interactions, combined with weak localization/antilocalization, can provide a possible explanation for the observed magnetoresistance.

DOI: 10.1103/PhysRevB.99.035408

I. INTRODUCTION

Since its discovery in 2004 [1], the two-dimensional electron gas (2DEG) at $SrTiO_3$ (STO)-based complex oxide interfaces has proven to be a fertile ground for the study of a great variety of physical phenomena [2–11]. The electronic structure of these systems is characterized by the presence of multiple, anisotropic bands at the Fermi surface [12–14], multivalent transition metal ions, a high degree of electronic correlations, and the breaking of inversion symmetry. This structure can be modified due to the ease of doping with oxygen vacancies [15–17] as well as other cations, the propensity to electronic and structural reconstructions and phase transitions, and strain [18,19]. Additionally, the high dielectric constant of STO, which can be tuned by an electric gate voltage V_g, allows for an *in situ* modulation of sample properties [20]. All these factors make for a complicated phase space, with phenomena including superconductivity [3,4,21,22], superconductor-insulator transitions [23,24], charge ordering [25], and magnetic behavior [2,8,9,11,26,27].

An important goal is to understand what interactions within STO-based 2DEGs lead to these varied behaviors, and how we can tune a particular physical parameter to control the interactions. Magnetoresistance (MR) studies in fields perpendicular and parallel to the 2DEG, in conjunction with temperature dependence measurements, are often used to shed light on the band structure and unravel the different mechanisms in a system, which typically show different dependencies on magnetic field scale, field orientation, and temperature. However, the situation in the case of STO-based 2DEGs is not straightforward, owing to the many degrees of freedom this electronic system possesses. The mobility and density of the multiple types of carriers present at the Fermi surface, which originate from the interfacial Ti $3d$ t_{2g} orbitals of STO [12,28], can be tuned by V_g, and the magnetic interactions between localized moments and/or itinerant carriers can be modified as a result [9,29,30]. The strong electron-electron interactions (EEI) [10,31,32], superconductivity [3,4], as well as spin-orbit interaction (SOI) [5–7] in the system are also controlled by V_g. Finally, the inherent disorder in the system, which gives rise to localization [5,33], is also dependent on V_g. All these phenomena contribute to sample resistivity at low temperatures, and must be accounted for when trying to understand transport in this system.

So far, research efforts have mainly focused on the (001) oriented STO-based 2DEGs. However, the (110) and (111) oriented heterostructures have recently been shown to host 2DEGs with fascinating properties [17,34–38]. In particular, the (111) oriented system is interesting owing to the hexagonal symmetry of the Ti $3d$ t_{2g} orbitals, and has been theoretically predicted to show topological physics [14,28,39,40]. Experimental work on (111) $LaAlO_3$/STO (LAO/STO) has revealed some peculiar features of transport, different from observations of (001) LAO/STO: the presence of intriguing anisotropies in many transport properties depending on the in-plane direction of transport [17,35,37,38], the presence of holelike carriers participating in transport especially at lower values of V_g [17,35–38], and a possible nematic phase [25]. All these properties were found to be tunable with oxygen vacancies [17,25]. Recently the SOI in (111) LAO/STO has been found to show a nonmonotonic dependence on V_g [6], as opposed to the well studied increase in the strength of SOI

*v-chandrasekhar@northwestern.edu

at larger positive values of V_g in the case of (001) LAO/STO [5,7].

We have previously studied the MR in perpendicular fields B in a different (111) oriented system: the 2DEG in (111) $(La_{0.3}Sr_{0.7})(Al_{0.65}Ta_{0.35})O_3$/STO (LSAT/STO) heterostructures [30,41]. LSAT has a 1% lattice mismatch with STO in comparison to the 3% lattice mismatch between LAO and STO. This gives rise to a smaller strain in the LSAT/STO system as compared to the more widely studied LAO/STO system, which can lead to higher carrier mobilities, as has already been shown in the case of (001) oriented systems [19,42,43]. The (111) LSAT/STO samples we studied also indicated the presence of a clean, high mobility 2DEG, as evidenced by a perpendicular MR of over 200% at $B \sim 10$ T, and a large residual resistance ratio of about 100 [30,41], which are both much larger than typical values reported so far for (111) LAO/STO samples [36]. Unlike in the case of (111) LAO/STO, we found no evidence of any systematic anisotropy dependent on the in-plane crystal directions in (111) LSAT/STO samples we studied, nor did we find any clear evidence of superconductivity down to ~40 mK [30], although it is possible that these properties can be tuned using different annealing treatments, as reported earlier for (111) LAO/STO samples [17]. We have also shown qualitatively that the SOI in the (111) LSAT/STO 2DEG *increases* as V_g is reduced [41], in contrast with what has been observed in the case of (001) STO-based 2DEGs [5], and that at milli-Kelvin temperatures, ferromagnetic order, characterized by hysteresis in the MR, emerges as the SOI becomes stronger at low values of V_g [30].

In this paper we discuss the quantitative analysis of the MR in high mobility STO-based 2DEGs, and in (111) LSAT/STO in particular. The observed high carrier mobility in our sample makes (111) LSAT/STO an ideal case study of the general (111) STO-based 2DEGs. We argue that obtaining quantitative values of the phase coherence length l_ϕ and the spin-orbit scattering length l_{so} is complicated by the possible presence of magnetic scattering and EEI, which result in an excess negative MR.

The rest of the paper is organized as follows: In Sec. II we review the various mechanisms that contribute to the resistivity of STO-based 2DEGs, along with their field and temperature dependencies. In Sec. III we describe our sample fabrication and measurement methods, and in Sec. IV we present the analysis of our MR data on (111) LSAT/STO. We show that we can fit our data up to $B \sim 3$ T in terms of weak localization/antilocalization corrections, by accounting for a background term which is second order in B. This background term comes from a combination of a positive MR due to the classical orbital contribution, and a negative MR that is quadratic at low fields and saturates at high fields, likely caused by magnetic scattering and EEI effects, which can be positive or negative. We quantitatively demonstrate that SOI in the (111) LSAT/STO 2DEG increases, and the phase coherence length decreases, with decreasing V_g.

II. CONTRIBUTIONS TO RESISTANCE

For STO-based 2DEGs, the sheet resistance R which depends on carrier density n and mobility μ as $R = 1/ne\mu$, can change by orders of magnitude when V_g is changed from large positive values to negative values (typically a few tens of volts to hundreds of volts, both positive and negative). In contrast, the Hall coefficient $R_H = 1/ne$ typically changes only by less than a factor of 2 or 3 [7,17,44]. This suggests that the change in resistance as a function of V_g is a result of a large change in carrier mobilities, which depend on scattering time τ and effective mass m^* as $\mu = e\tau/m^*$, rather than a change in carrier densities. This trend in R and R_H, which is a common feature of STO-based 2DEGs [5,8,17], is also observed in our sample [41] and warrants further investigation to understand the causes of the drastic change in μ, or equivalently, in τ.

For STO-based 2DEGs in general, the sheet resistance is known to show a minimum at a temperature of a few Kelvin, increasing in value as temperature is lowered further, before finally either saturating, or vanishing if the sample undergoes a superconducting transition [2,3,19,30,45] depending on growth conditions and the particular value of V_g. Hence the MR at sub-Kelvin temperatures for different values of V_g can give us important information about the scattering mechanisms that lead to the aforementioned drastic changes in R as a function of V_g, given that these changes are amplified at lower values of T.

Various scattering processes exist in a system, and are modulated by factors such as T, V_g, and B. We now look at the contributions to R due to each of these processes, and discuss, in the context of STO-based 2DEGs, how they affect $R(T, B)$ as the disorder, dimensionality, SOI, and the multiband nature of the system is changed.

A. Magnetic field independent contributions

Drude contribution (R_0): In metallic systems, the sheet resistance at zero field R_0, independent of T and B, is the Drude contribution, caused by the elastic scattering of carriers off static impurities and surfaces, and can be calculated in terms of the transport scattering time (τ), carrier density (n), and carrier mass (m^*). In 2D systems, in which conductivity is the same as conductance, the Drude contribution can be written as $R_0 = m^*/ne^2\tau$, where n is the areal charge density. If contributions due to other mechanisms are small compared to R, then the resistance R can be approximated as R_0 for the purpose of determining τ. However, in a real system where other contributions are substantial and difficult to pry apart, it is unclear that the measurement of R at any given temperature gives us the value of R_0. In the case of STO-based 2DEGs, this is especially a problem in the case of measurements at negative values of V_g, for which resistance changes rapidly as a function of T at the low temperatures of interest, and the Drude picture may not apply. For our (111) LSAT/STO sample, this can be seen clearly from Fig. 1, where for $V_g = -40$ V, R changes by over 15% between $T = 500$ and 50 mK, whereas R changes by only about 1% for $V_g = 100$ V in the same temperature range. We found that the situation is amenable to analysis for the range of V_g studied in more detail in this paper, i.e., $V_g \geqslant 60$ V, where we observed that R changes by less than 5% over the temperature range of interest for our sample.

The carrier density n is usually estimated using Hall data. Hall data in STO-based interfaces are electronlike, and show

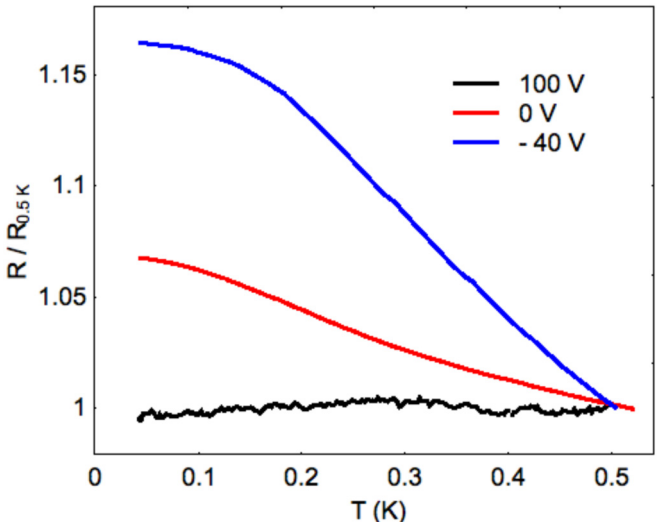

FIG. 1. R as a function of T for $V_g = 100$, 0, and -40 V. R has been normalized to its value at $T = 500$ mK. The absolute values of R at $V_g = 100$, 0, and -40 V at $T = 50$ mK are 76 Ω, 7.03 kΩ, and 33.34 kΩ, respectively.

nonlinear behavior, especially at higher values of V_g. This has been interpreted as evidence of multicarrier transport [13]. At lower values of V_g holelike carriers are also believed to play a role in the case of (111) oriented STO-based systems [17,30]. Hence the estimate of n obtained from Hall measurements may not be a good approximation for these systems. This in turn introduces uncertainty in the straightforward determination of τ, which complicates the determination of other transport parameters, namely, the Fermi wave number $k_F = \sqrt{2\pi n}$, Fermi velocity $v_F = \hbar k_F/m^*$, mean free path l, and the diffusion constant $D = v_F l/2$ for two-dimensional systems.

The effective carrier mass m^* is typically obtained from angle resolved photoemission spectroscopy (ARPES) measurements. ARPES studies on vacuum cleaved (111) STO have revealed highly anisotropic effective masses of electrons from the Ti $3d$ t_{2g} orbitals of interest, with a heavy (light) mass of 1.8 m_e (0.27 m_e) along the $[1\bar{1}0]$ direction, and a heavy (light) mass of 8.67 m_e (0.33 m_e) along the $[\bar{1}\bar{1}2]$ direction, with m_e being the bare electron mass [14]. An estimate for the cyclotron m^* can also be obtained from an analysis of Shubnikov–de Haas (SdH) data. In the case of our (111) LSAT/STO sample, we do not see enough SdH oscillations within the range of field available to us (10 T) to get a reliable estimate of m^* [41]. The absence of reliable estimates of m^* also obfuscates the determination of τ and the other parameters as described above.

Contribution due to phonon scattering $[\Delta R_{\rm ph}(T)]$: Inelastic scattering of electrons off phonons leads to a contribution with a power-law temperature dependence. The electron-phonon contribution is proportional to T^5 in the clean limit in the case of simple isotropic metals, or proportional to T^3 if Umklapp scattering is dominant [46]. Other powers are also possible if multiple types of scattering mechanisms are present [47]. We note that these contributions are not expected to play a role in the temperature range under study in this paper, since these scattering mechanisms are frozen out to a large extent at very low temperatures. In STO-based systems, many experiments have identified a T^2 dependence of R [32,48,49], attributed to phonon-mediated electron-electron scattering, or electron-electron scattering in the presence of multiple bands.

Contribution due to charged impurities $[\Delta R_{\rm ion}(T)]$: Charged impurities such as oxygen vacancies are a common occurrence in STO. These occur, for example, when the system is annealed in a reducing atmosphere, causing the removal of neutral oxygen atoms from the crystal. This leaves behind two extra electrons in the crystal. Near the interface, these oxygen vacancies form a donor level just below the conduction band (which is composed of $3d$ orbitals) of the system. The extra electrons can be excited into the conduction band if the temperature is high enough, and participate in transport. However, as T is reduced, electrons can drop back into the donor level, in effect being trapped by the positively charged oxygen vacancy sites. These charge traps are known to have activation temperatures T_A ranging from a few Kelvin to a few tens of Kelvins [16]. The concentration of these charged impurities decreases exponentially with increasing temperature on the scale of T_A. Also, the screening of these impurities decreases with increasing temperature, since the dielectric permittivity of STO, which is also a function of V_g, decreases with increasing temperature [50]. Scattering of electrons off these partially screened charged impurities leads to the contribution $\Delta R_{\rm ion}(T)$, which when combined with the change in resistivity caused by the inelastic mechanisms described in the previous paragraph, can lead to a resistance minimum at intermediate temperatures, with low-temperature saturation, that is commonly observed in STO based 2DEGs [32]. This mechanism may be present in combination with the Kondo mechanism, which is typically used in order to describe the observed resistance minimum in these systems [2,45], and which will be discussed later.

B. Magnetic field dependent contributions

Classical orbital contribution $[\Delta R_{\rm cl}(T, B)]$: A magnetic field perpendicular to the 2DEG causes an increase in path length and backscattering of electrons due to orbital effects. If only electronlike (or holelike) carriers from closed bands participate in transport in a clean system (with one dominant carrier mobility), $\Delta R_{\rm cl}(T, B)$ is proportional to $B^2 \sim (\omega_c\tau)^2$ for low fields ($\omega_c\tau < 1$), where $\omega_c = eB/m^*$ is the cyclotron frequency, while the MR saturates at high fields ($\omega_c\tau > 1$). In the case of STO-based systems, a quasilinear behavior is typically observed at high fields [30,51], indicative of some degree of hole transport, or disorder (large spread in carrier mobility) in the 2DEG [52]. In high-mobility STO-based 2DEGs [51], for large positive values of V_g where multiple bands contribute to transport, this $\Delta R_{\rm cl}(B)$ can be very large, comparable to any low-field corrections to the MR at fields as small as a few 100 mT [41], and must be taken into consideration as a background while analyzing the low-field MR. As the scattering time τ increases with decreasing temperature, this contribution increases with decreasing T.

Contributions due to magnetic scattering $[\Delta R_{\rm mag}(T, B)]$: Going from higher to lower values of V_g, the size of $\Delta R_{\rm cl}(B)$ is observed to reduce considerably, and in some cases a

negative MR emerges at the lowest values of V_g [13,30]. This MR is seen to remain negative even at the highest values of B studied. One of the causes of negative MR is the presence of magnetic scattering in the system. STO-based 2DEGs are known to show a wide range of magnetic phenomena, ranging from Kondo-like behavior caused by dilute magnetic scatterers in the system, to spin glasses, to a full ferromagnetic phase at the highest concentration of magnetic scatterers [29]. What is more, these three regimes may coexist in the 2DEG owing to a disordered distribution of magnetic scatterers. For all these regimes, however, a negative isotropic MR has been predicted and observed in many systems including STO-based 2DEGs [2,53,54]. This negative contribution to the MR, $\Delta R_{\rm mag}(T, B)$, which can be large, is proportional to B^2 for smaller fields, and saturates at higher fields greater than those required to saturate the magnetic moments. This negative MR must also be considered on a similar footing as the positive $\Delta R_{\rm cl}(B)$ in order to analyze the low-field corrections.

The temperature dependence of resistivity due to the presence of magnetic scatterers depends on the whether the magnetic moments are in the dilute or the spin glass limit. In both situations the resistivity increases logarithmically as temperature is decreased, as conduction electrons scatter off partially screened magnetic moments. If the temperature is lowered below the characteristic Kondo temperature of the system, the moments are fully screened, and a saturation in resistance is observed. If, however, the concentration of magnetic moments is high, and if the temperature is low enough that the thermal energy is smaller than the strength of interaction between individual magnetic moments, the moments start to freeze out, leading to a spin-glass phase, wherein the sample resistance can even decrease as temperature is lowered [55]. Thus the presence of magnetic moments in STO-based 2DEGs can be invoked to explain some of the observed T and B dependencies in this system.

It was discussed earlier that scattering of conduction electrons off ionic impurities can give a similar temperature dependence as the scattering of conduction electrons off magnetic moments. In principle, it should be possible to tell these two mechanisms apart by measuring the temperature dependence of resistance while applying a magnetic field. $\Delta R_{\rm ion}(T)$ should remain unaffected by B, while in the case of $\Delta R_{\rm mag}(T, B)$, the resistance minimum and low-temperature saturation should progressively disappear for higher values of B. However, the presence of localization corrections and EEI corrections (to be discussed later) also can give rise to a difference in the temperature dependence of resistivity for different values of B. Another way would be to look for a peak in specific heat of the sample near the estimated Kondo temperature, however, to our knowledge, this technique has not been used so far in the case of STO-based 2DEGs.

Single particle localization contributions [$\Delta R_{\rm loc}(T, B)$]: In two dimensions in the presence of disorder, and in the absence of SOI, all electronic states are localized at zero temperature [56]. If disorder is strong, i.e., $k_F l < 1$ or equivalently, $R > R_Q = 25.812\ {\rm k}\Omega/\square$, which is the quantum of resistance, then $\Delta R_{\rm loc}(T, B)$ increases exponentially as a function of T [57]. For our sample, even at the lowest value of V_g studied, i.e., $V_g = -40$ V, R at $T = 50$ mK is $\sim 33\ {\rm k}\Omega/\square$, only marginally greater than R_Q.

In the regime of R for our sample, the predictions of the weak localization theory, which assumes a diffusive system and employs perturbative techniques to derive single-particle corrections to the conductivity resulting from the constructive interference of coherently backscattered carriers, are generally valid [58]. In two dimensions, weak localization predicts a logarithmic increase in resistance as T is reduced as given by Eq. (1) [57]:

$$\Delta R_{\rm loc}(T, 0) = -\frac{R_0^2}{2\pi^2\hbar/e^2}\ p\ \ln\frac{T}{T_0}, \tag{1}$$

where $T_0 = \hbar/k_B\tau$. The effect is caused by an increase in the phase coherence time τ_ϕ with decreasing temperature, which typically goes as T^{-p} [57], where p depends on the mechanism of decoherence. An applied magnetic field perpendicular to the 2DEG also impedes the coherent interference of the backscattered electron waves, and leads to a MR. The sign and magnitude of this MR depends on not just τ_ϕ, but also on $\tau_{\rm so}$, the spin-orbit scattering time, and τ_s, the spin-flip scattering time. The form is also dependent on the type of SOI present in the system, i.e., whether it has a cubic or a linear dependence on momentum [59,60].

In a multiband system, when τ_ϕ is long enough that electrons are scattered frequently between the different bands and different parts of the Fermi surface before losing phase coherence, Rainer *et al.* [61] showed that single band theories of weak localization [62,63] are valid, and the characteristic time/length scales calculated from such theories give the averages of these parameters over the relevant bands. This idea has been widely used in earlier analyses of the MR in STO-based 2DEGs [5–7]. In the particular multiband system of (001) oriented STO-based 2DEGs, the orbital ordering of the t_{2g} bands was considered by Kim *et al.* [60], who calculated conductivity corrections based on a linear-in k Rashba SOI in the d_{xy} bands and a cubic-in k Rashba SOI in the $d_{yz;zx}$ bands. No such calculations have been done yet for the orbital ordering observed in (111) oriented STO-based systems. If SOI is substantial, then Zeeman effects can play a role as well, with the electron g factor of the 2DEG as an additional parameter [62]. Finally, the exact form of the T and B dependencies are dictated by the dimensionality of the system with respect to weak localization, i.e., if the associated length scale for decoherence $l_\phi = \sqrt{D\tau_\phi}$ is greater than the film thickness d, then the film is in the two-dimensional limit.

Despite the complexity of the various theories, it is clear that SOI is an antilocalizing mechanism, since the spin rotation caused by SOI leads to an increase in the destructive interference of coherently backscattered carriers. Hence an applied B, which causes decoherence, causes a negative MR in the absence of strong SOI, and a positive MR in the presence of a strong SOI. The role of magnetic scattering is also to cause decoherence [64]. The changes in conductivity due to weak localization/antilocalization are of the order of $\sigma_0 = 2e^2/h$, while the field scales of the effects B_α depend on D and the relevant scattering time τ_α as $B_\alpha = \hbar/4eD\tau_\alpha$. Estimates of B_α can be obtained by fitting to equations which describe $\Delta R_{\rm loc}(T, B)$ in terms of these characteristic field

scales, such as the theory of Hikami *et al.* [63]:

$$\frac{\Delta R_{\rm loc}(T,B)}{R_0} = \frac{R_0}{2\pi^2\hbar/e^2}\left[-\frac{3}{2}\Psi\left(\frac{1}{2}+\frac{B_2}{B}\right) + \frac{1}{2}\Psi\left(\frac{1}{2}+\frac{B_1}{B}\right)+\ln\frac{B_0}{B}\right]. \quad (2)$$

Here $B_1 = B_\phi + 2B_s$, while $B_2 = B_\phi + (4/3)B_{\rm so} + (2/3)B_s$, and B_0 is the field associated with the elastic scattering time τ. When analyzing the normalized differential MR data, the elastic field B_0, and hence the elastic time τ, which is difficult to determine experimentally, drops out of the equation, as we shall discuss in Sec. IV. In the context of STO-based 2DEGs, it is difficult to obtain reliable estimates of the diffusion constant D and the scattering time τ of the system as discussed earlier, hence we describe $\Delta R_{\rm loc}(T, B)$ in terms of characteristic length scales l_α instead of the characteristic times τ_α, with $l_\alpha^2 = \hbar/4eB_\alpha$. The temperature dependence of magnetic scattering in this system is also unknown. To minimize the number of fit parameters in the analysis, we ignore B_s, which is the contribution of magnetic scattering, as well as the Zeeman effect to weak localization corrections, and use the form in Eq. (2) derived by Hikami, Larkin, and Nagaoka, which considers the effect of SOI only as a scattering rate, without using the forms specific for linear or cubic SOI.

The corrections due to localization are expected to decrease with increasing B, and completely die out at $B \sim \hbar/l^2e$ [64].

Contributions due to EEI in the diffusive limit $[\Delta R_{\rm EEI}(T, B)]$: EEI effects contribute to the sample resistance in a number of ways. Large angle inelastic collisions in the ballistic limit contribute to the T^2 dependence of $\Delta R_{\rm in}(T)$ discussed earlier. Small as well as large angle collisions can modify single particle lifetimes of electrons and cause the decoherence of electron wave functions, thus affecting τ_ϕ which in turn affects the localization corrections. On the other hand, many-body EEI effects in the diffusive limit can cause a change in the density of states of the 2DEG, and lead to the following corrections to the conductivity [65]:

$$\Delta\sigma_{\rm EEI}(T,B) = \frac{e^2}{\hbar}\frac{1}{4\pi^2}\left(2-\frac{3F}{2}\right)\ln\left(\frac{k_BT\tau}{\hbar}\right) - \frac{e^2}{\hbar}\frac{1}{4\pi^2}Fg_2\left(\frac{g\mu_BB}{k_BT}\right) - \frac{e^2}{\hbar}\frac{1}{4\pi^2}g_1(T)\Phi_2\left(\frac{2DeB}{\pi k_BT}\right). \quad (3)$$

Here the first term is the field-independent exchange and singlet Hartree contribution of the particle-hole channel, the second term is the triplet Hartree contribution, while the third term is the orbital contribution due to the particle-particle channel [57]. F and $g_1(T)$ are both related to the screened Coulomb potential. Since typically $|g_1(T)| \ll 1$, this term is usually ignored. F is typically of the order of unity, and hence the first two terms of the equation must be considered in our analysis.

The second term gives a negative correction to the conductivity, and hence a positive $\Delta R_{\rm EEI}(B)$. $g_2(T, B)$ has a functional form, $\sim 0.084(g\mu_BB/k_BT)^2$ for $g\mu_BB/k_BT \ll 1$ and $\sim \ln(g\mu_BB/k_BT)/1.3$ for $g\mu_BB/k_BT \gg 1$. For $T = 100$ mK and assuming $g = 2$, this field scale is about $B = 75$ mT.

The first correction to the conductivity, although independent of B, leads to a contribution to the resistivity which is quadratic in B, which we can obtain by inverting the conductivity tensor, and noting that EEI corrections also lead to a contribution in the Hall coefficient, which are twice the corrections to the resistivity due to EEI effects. These corrections, calculated by Houghton *et al.* [66], are given as

$$\Delta R_{\rm EEI}^{\rm ex}(T,B) = \frac{-m^*}{4\pi^2\hbar n\tau}\left(2-\frac{3F}{2}\right)[1-(\omega_c\tau)^2]\ln\left(\frac{k_BT\tau}{\hbar}\right). \quad (4)$$

As we noted earlier, $\omega_c\tau$ in our high mobility sample, especially at large positive values of V_g, can be substantial even at small values of B. This discussion makes is clear that for analyzing low field data, we must consider the effect of EEI along with localization. Usually the procedure is to isolate the EEI contributions by considering large fields, at which localization corrections are negligible. However, for the high mobility STO-based 2DEGs, the classical contribution rapidly increases with increasing field, making the resolution of EEI contributions in this manner impossible. Another way to isolate EEI is by measuring MR in fields parallel to the 2DEG, since this would eliminate the large positive background of $\Delta R_{\rm cl}(B)$. However, in the case of STO-based 2DEGs, this runs into difficulties as one still has to contend with a negative quadratic background from magnetic scattering. It is also possible in principle to isolate the EEI contribution using R vs T data, in cases where the $\Delta R_{\rm EEI}^{\rm ex}(T, B)$ is negligible due to $\omega_c\tau$ being very small. Since EEI leads to a logarithmic increase in R as temperature is lowered, similar to weak localization effects, this is usually done by measuring R vs T in the presence of a magnetic field larger than that required to suppress localization effects. However, the application of a magnetic field would also affect the $\Delta R_{\rm mag}(T, B)$ contribution in STO-based 2DEGs, making the isolation of EEI effects difficult. We do expect EEI effects in STO-based 2DEGs to be substantial especially at the low temperatures of study, given that the carriers originate from the narrow $3d\ t_{2g}$ orbitals of Ti.

Contributions due to superconducting fluctuations $[\Delta R_{\rm SC}(T, B)]$: Finally, we discuss the contribution due to superconducting fluctuations. STO-based 2DEGs commonly show a superconducting transition below about 300 mK. In the vicinity of a superconducting transition, Aslamazov-Larkin [67] corrections to the conductivity, which are caused by fluctuating Cooper pairs, and Maki-Thompson [68] corrections, which are caused by the coherent scattering of carriers off the fluctuating Cooper pairs, can be important, depending on sample cleanliness and measurement temperature [69]. This transition was not observed in the case of our (111) LSAT/STO sample. Our sample does show a very slight drop in resistance below about 300 mK for $V_g \geqslant 60$ V (see Fig. 1), but it is not clear whether this slight drop is due to superconducting fluctuations, or due to other contributions to the resistivity, such as antilocalization corrections or magnetic scattering. Due to the absence of

a full superconducting transition, we ignore this effect in our analysis, however, we note that it must be taken into consideration in samples which do show a superconducting transition.

III. SAMPLE FABRICATION AND MEASUREMENT

Pulsed laser deposition was used to deposit 12 monolayers of LSAT epitaxially on (111) oriented STO at a partial oxygen pressure of 10^{-4} Torr [19]. No post growth annealing step was performed. Using a combination of photolithography and Ar ion milling, the 5 mm × 5 mm LSAT/STO chip was patterned to make four Hall bars, 100 μm wide and 600 μm long. Two of the Hall bars had their lengths oriented along the $[1\bar{1}0]$ crystal direction and the other two had their lengths oriented along the $[\bar{1}\bar{1}2]$ crystal direction. Ti/Au was deposited on contact pads, and Al wirebonds were made to allow for a four-probe measurement configuration of transverse and longitudinal resistance. The sample was attached to a copper puck using silver paint, with care being taken to keep the silver paint off the sides of the sample, which enabled the application of a back gate voltage. The sample was measured in an Oxford Kelvinox MX100 dilution refrigerator. Standard lock-in measurement techniques were used to measure the differential resistance, with an ac frequency of 3 Hz, and an ac current ∼100 nA. We have shown in an earlier publication [41] that transport in (111) LSAT/STO samples grown under these conditions does not exhibit the directional anisotropy which characterizes transport in (111) LAO/STO [17]. Hence we only discuss data obtained on a single Hall bar, oriented along the $[\bar{1}\bar{1}2]$ direction, other Hall bars showing qualitatively similar results. On initially cooling down to $T = 50$ mK, V_g was swept multiple times over the entire range, 100 to −40 V, in order to ensure that the changes in properties due to changes in V_g are reproducible, going always from higher to lower values of V_g.

As discussed earlier, R as a function of T can be nonmonotonic for STO-based 2DEGs. Figure 1 shows the variation of R_s with T for three different values of V_g, normalized to the respective values of R_s at $T = 0.5$ K. The data show low T increase and saturation of resistance for $V_g = 0$ and −40 V. For $V_g = 100$ V, saturation of resistance is observed at the lowest temperature but full superconductivity is not observed. We study the MR below $T = 750$ mK for $V_g \geqslant 60$ V, since in this range of V_g, the hysteretic MR associated with the low-temperature ferromagnetic phase is absent [30], hence allowing the analysis of the low field MR in terms of weak localization.

IV. MAGNETORESISTANCE ANALYSIS

At milli-Kelvin temperatures, the $\Delta R_{\rm ph}(T)$ and $\Delta R_{\rm ion}(T)$ contributions freeze out, hence they can be ignored in our analysis. $\Delta R_{\rm SC}(T, B)$ is also ignored since we do not see superconductivity in our sample. Given the difficulties in isolating contributions due to magnetic scattering effects and EEI effects in these STO-based 2DEGs, we are left with the following equation for $R(T, B)$:

$$R(T, B) = R_0 + \Delta R_{\rm cl}(T, B) + \Delta R_{\rm mag}(T, B) + \Delta R_{\rm EEI}(T, B) + \Delta R_{\rm loc}(T, B). \quad (5)$$

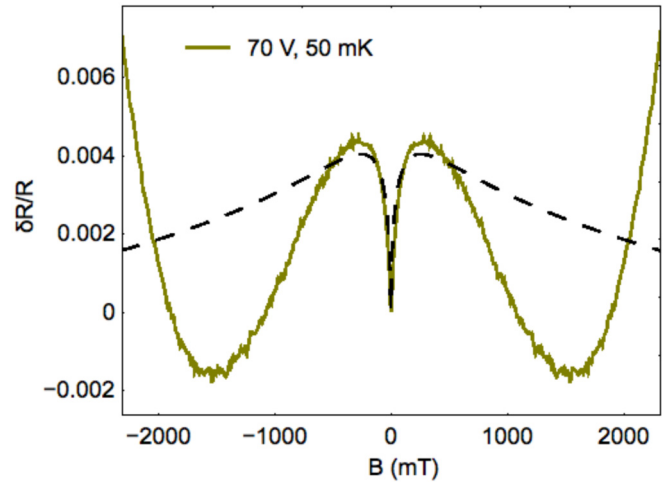

FIG. 2. $\delta R/R$ vs B at $V_g = 70$ V and $T = 50$ mK. The dashed line is a fit to Eq. (7).

For $V_g \geqslant 60$ V, as discussed earlier, we can approximate R as R_0, and hence write the differential MR as

$$\frac{\delta R(T, B)}{R} = \frac{R(T, B) - R(T, B = 0)}{R}, \quad (6)$$

which has the terms $\Delta R_{\rm loc}(T, B) - \Delta R_{\rm loc}(T, B = 0)$. From Eq. (2), and noting that the asymptotic form for $\Psi(1/2 + B_\alpha/B)$ as $B \to 0$ is $\ln(B_\alpha/B)$, one arrives at the following form for the differential localization correction [46]:

$$\frac{\delta R_{\rm loc}(T, B)}{R} = -\frac{3}{2} f(B, B_2) + \frac{1}{2} f(B, B_1). \quad (7)$$

Here the first term is the triplet Cooperon contribution while the second term is the singlet Cooperon contribution, and the function f is given as

$$f(B, B_\alpha) = \frac{R}{2\pi^2 \hbar/e^2}\left[\Psi\left(\frac{1}{2} + \frac{B_\alpha}{B}\right) - \ln\left(\frac{B_\alpha}{B}\right)\right]. \quad (8)$$

Here we note that the elastic field $B_0 = \hbar/4eD\tau$ does not feature in the above equations, thus removing the dependence on τ, which is difficult to determine, as we discussed earlier. Figure 2 shows $\delta R/R$ for $V_g = 70$ V and $T = 50$ mK, along with a fit to Eqs. (7) and (8). We see that attempting to fit the low field increase in the MR, which is associated with the presence of a strong SOI, leads to an extremely poor fit at higher fields. This excess negative MR cannot be explained by the classical quadratic background alone since that gives a positive MR. Hence, in our analysis, we use the following terms to account for the background due to the classical MR, magnetic scattering, as well as EEI:

$$\frac{\delta R_{\rm BG}(T, B)}{R} = AB^2 - \frac{CB^2}{D + EB^2}. \quad (9)$$

Both the positive classical orbital background, and the EEI contribution due to exchange and singlet Hartree terms described by Eq. (4), which can be positive or negative, are quadratic in field, and are accounted for by the first term of Eq. (9). Both these contributions are proportional to $(\omega_c\tau)^2$, hence we expect them to be stronger for larger values of V_g at which ω_c values are larger. Also, both contributions

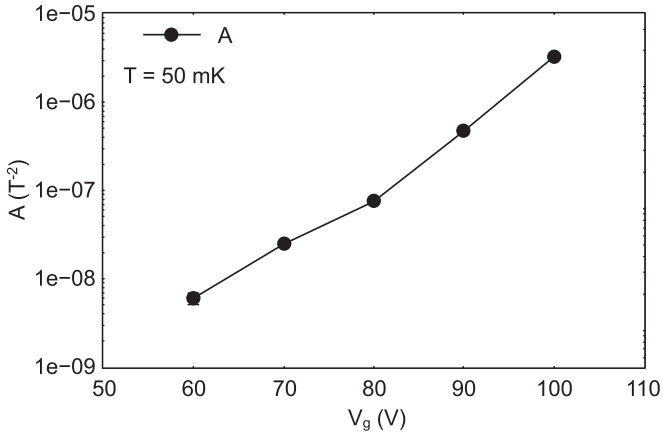

FIG. 3. Variation of the parameter A with V_g at $T = 50$ mK.

can be T dependent due to changes in τ, and the exchange and the singlet Hartree contribution of EEI, varies logarithmically with T. Despite this, we found experimentally that our background was well described by assuming a temperature independent parameter A. This leads us to conclude that the effective temperature dependence of τ is likely to be small in the temperature range of interest. Additionally, if the singlet EEI contribution is positive, it appears to be much smaller than the classical orbital contribution since A appears to be independent of T. We can make no such comparison if the singlet EEI contribution is negative. Figure 3 shows the variation of parameter A with V_g.

The second term in Eq. (9) is quadratic at small fields and saturates at higher fields. This term might arise from the negative contribution due to magnetic scattering discussed earlier. Contributions to EEI which come from the triplet exchange interactions, described by the second term of Eq. (3), are quadratic at smaller fields, and logarithmic at larger fields. This can also be roughly approximated by the second term of Eq. (9). The coefficients C, D, and E were allowed to vary with T, since the contributions due to magnetic scattering and EEI can be temperature dependent. Figure 4 shows the variation of these three parameters with T and V_g. Note that due to the form of the second term in Eq. (9), the values of the parameters C, D, and E can vary by some multiplicative factor. To see how the background terms from Eq. (9) and the weak localization term from Eq. (7) contribute towards the measured MR signal, see Fig. 5.

B_{so} was also held constant since it is expected to be independent of T, given that the factors contributing to SOI, namely, band structure effects, atomic SOI, and the electric field due to V_g and the confinement potential are expected to be constant in this temperature range. Zeeman and magnetic scattering effects on weak localization were ignored.

Figure 6(a) shows the MR data, at various values of T for $V_g = 60$ V, with fits to Eq. (7), along with a background given by Eq. (9). Figure 6(b) shows the variation of the extracted $l_\phi^2 \sim \tau_\phi$ as a function of T, for various values of V_g. We see that τ_ϕ increases as T is decreased for all V_g, and as expected, the increase is the largest for $V_g = 100$ V for which sheet resistance R is the smallest. The rate of increase in τ_ϕ also

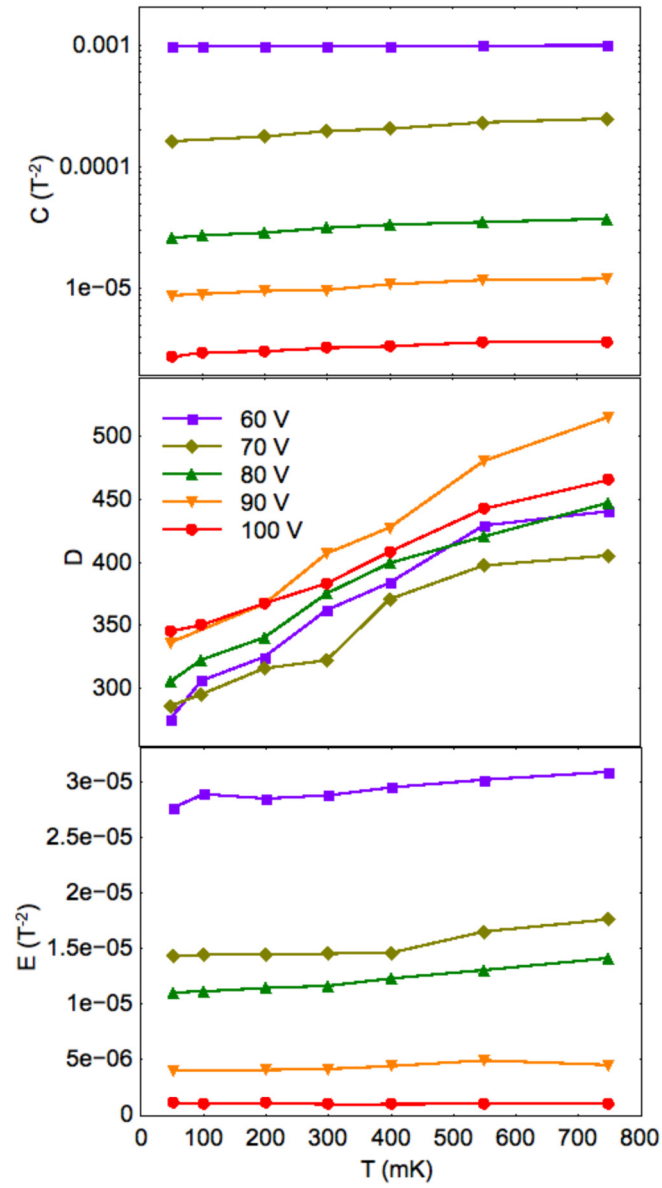

FIG. 4. Variation of the parameters C, D, and E with T at different values of V_g.

seems to slow down at lower values of T, with the biggest effect for $V_g = 60$ V, which has the largest R.

Figure 7(a) shows the MR for various values of V_g, measured at $T = 50$ mK. From these fits we obtained estimates for l_{so} and l_ϕ at $T = 50$ mK for values of V_g, which are plotted in Fig. 7(b). We see that l_ϕ, on the left axis, decreases as a function of V_g. This is as expected from the variation in sheet resistance with V_g, shown in the inset of Fig. 7(b). Curiously, many earlier experimental works on (001) LAO/STO have found that the values of l_ϕ or τ_ϕ changed relatively little over a large range of V_g explored, even though the sheet resistances varied by an order of magnitude or more [5,7]. We also note that the values of l_ϕ obtained from our calculations are quite large, in the range of several hundred nanometers, as opposed to values typically obtained in earlier studies of (001) oriented LAO/STO, which are in the range of tens of

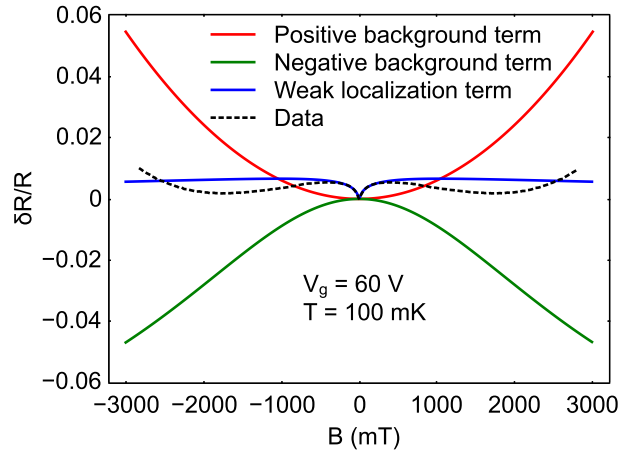

FIG. 5. Contributions due to the positive background term of Eq. (9), the negative background term of Eq. (9), and the WL term given by Eq. (7), along with the actual data, for $V_g = 60$ V and $T = 100$ mK.

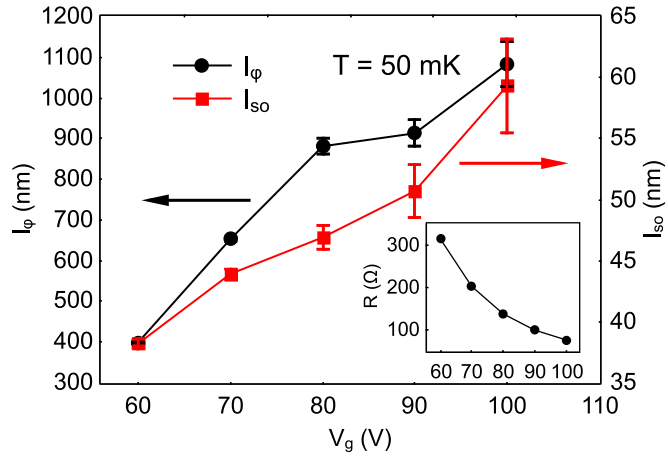

FIG. 7. (a) $\delta R/R$ vs B at $T = 50$ mK and various values of V_g. The dashed line is a fit to Eq. (7) with a background described by Eq. (9). (b) l_ϕ and l_{so} as a function of V_g for $T = 50$ mK. Inset shows the variation of the sheet resistance with V_g at $T = 50$ mK, with the vertical axis showing values in Ohms.

nanometers [5,7]. This could be an indication of the relatively clean nature of the LSAT/STO system, with its reduced strain. Direct comparison with the earlier report on (111) LAO/STO is not possible, since it studied the system in the regime of large values of sheet resistance ($\geqslant$0.8 kΩ) [6], while our studies are limited to the regime of high mobility and low sheet resistance ($\leqslant$0.3 kΩ). Figure 7(b) also clearly shows that l_{so} *decreases* with V_g, indicating that SOI becomes stronger as V_g is reduced. Further decrease in V_g below ~60 V at these temperatures leads into a ferromagnetic phase characterized by a hysteretic MR, as shown in our earlier report [30].

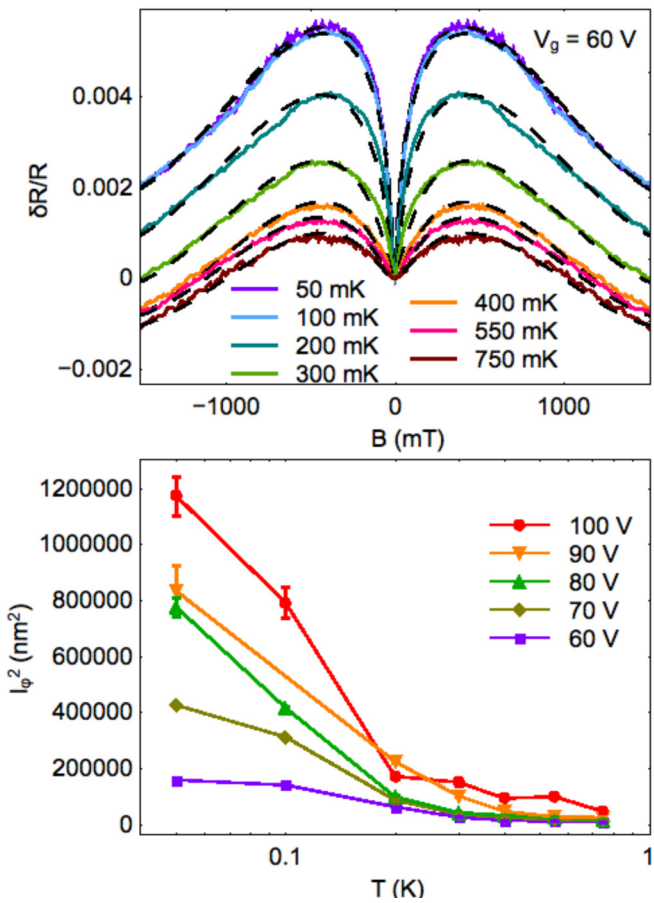

FIG. 6. (a) $\delta R/R$ vs B at $V_g = 60$ V and various T. The dashed line is a fit to Eq. (7) with a background described by Eq. (9). (b) l_ϕ^2 ($\sim\tau_\phi$) as a function of T on a logarithmic scale, for various V_g.

In order to understand this variation in SOI with V_g in the case of (111) LSAT/STO, which is opposite to the trend generally observed in (001) oriented LAO/STO, we begin by noting that in this system, the SOI can be either of the atomic or the Rashba type. Atomic SOI depends on the band filling in the $3d$ t_{2g} system, with the strongest effects seen at the bottom of otherwise degenerate bands [70]. In the case of (001) oriented STO-based systems, the d_{xy} band is the lowest in energy, whereas the $d_{yz,zx}$ bands are degenerate and higher in energy due to the breaking of interfacial symmetry at the interface. As increasing V_g causes these high energy bands to start filling, atomic SOI increases with increasing V_g [13]. On the other hand, density functional theory calculations have shown that in (111) oriented STO-based systems which experience a trigonal crystal field, the three $3d$ t_{2g} orbitals split into an e_g' doublet and an a_{1g} singlet [39,40]. In the case of systems with a compressive strain, such as (111) LSAT/STO, the e_g' doublet is lower in energy than the a_{1g} singlet, and hence one may expect the effects of atomic SOI to be stronger when only the lower bands are filled, i.e., at more negative values of V_g. As V_g is increased, carriers begin to be added to the higher energy band, decreasing the average value of l_{so} of the carriers.

The Rashba Hamiltonian is given as $H_R = \alpha(\hat{\mathbf{n}} \times \vec{\mathbf{k}}) \cdot \vec{\mathbf{S}}$. Here $\vec{\mathbf{S}}$ are the Pauli matrices, $\vec{\mathbf{k}}$ is the electron wave vector, and $\hat{\mathbf{n}}$ is the unit vector perpendicular to the 2DEG plane. Thus the Rashba SOI depends on the value of k_F, and hence hence one would expect SOI to increase with band filling, or equivalently, with V_g. The Rashba SOI coupling constant α is dependent on the magnitude of the atomic SOI [13], and hence would be expected to increase with decreasing V_g in

(111) LSAT/STO as per our earlier discussion. However, the Rashba SOI also depends on the gradient of the electric field experienced by the carriers, which depends on the value of V_g, as also on the confinement potential at the interface, which is dependent on whether the applied gate voltage is positive or negative [71]. It is unclear which of these effects dominate in determining the Rashba SOI in the system. It is clear however, that the overall effect of atomic and Rashba SOI increases with decreasing values of V_g.

V. CONCLUSIONS

We have shown that analysis of MR in STO-based 2DEGs must consider a variety of scattering phenomena which have complicated field and temperature dependence. The strong negative MR shown by our LSAT/STO sample suggests that magnetic scattering and EEI contributions must play a major role in determining MR. Analyzing our data in terms of these contributions in addition to a positive classical background and weak localization effects, leads us to conclude that SOI indeed gets stronger at smaller gate voltages, and may play a role in the ferromagnetic state that develops at these gate voltages. We note that we have neglected the contribution of magnetic scattering and Zeeman effect to the weak localization corrections. We have also neglected the fact that converting from resistance to conductance involves considering the Hall angle, which can lead to a 20% difference in the estimated value of conductance, and can affect the weak localization contribution.

ACKNOWLEDGMENTS

The US Department of Energy, Office of Basic Energy Sciences supported the work at Northwestern University through Grant No. DE-FG02-06ER46346. Work at NUS was supported by the MOE Tier 1 (Grants No. R-144-000-364-112 and No. R-144-000-391-114) and Singapore National Research Foundation (NRF) under the Competitive Research Programs (CRP Award No. NRF-CRP15-2015-01). This work utilized Northwestern University Micro/Nano Fabrication Facility (NUFAB), which is supported by the State of Illinois and Northwestern University.

[1] A. Ohtomo and H. Y. Hwang, A high-mobility electron gas at the $LaAlO_3/SrTiO_3$ heterointerface, Nature (London) **427**, 423 (2004).

[2] A. Brinkman, M. Hujiben, M. van Zalk, J. Hujiben, U. Zeitler, J. C. Mann, W. G. van der Wiel, G. Rijnders, D. H. A. Blank, and H. Hilgenkamp, Magnetic effects at the interface between non-magnetic oxides, Nat. Mater. **6**, 493 (2007).

[3] N. Reyren, S. Thiel, A. D. Caviglia, L. Fitting Kourkoutis, G. Hammerl, C. Richter, C. W. Schneider, T. Kopp, A.-S. Rëtschi, D. Jaccard, M. Gabay, D. A. Muller, J.-M. Triscone, and J. Mannhart, Superconducting interfaces between insulating oxides, Science **317**, 1196 (2007).

[4] S. Thiel, G. Hammerl, A. Schmehl, C. W. Schneider, and J. Mannhart, Tunable quasi-two-dimensional electron gases in oxide heterostructures, Science **313**, 1942 (2006).

[5] A. D. Caviglia, M. Gabay, Gariglio, N. Reyren, S. C. Cancellieri, and J. M. Triscone, Tunable Rashba Spin-Orbit Interaction at Oxide Interfaces, Phys. Rev. Lett. **105**, 236802 (2010).

[6] P. K. Rout, E. Maniv, and Y. Dagan, Link between the Superconducting Dome and Spin-Orbit Interaction in the (111) $LaAlO_3/SrTiO_3$ interface, Phys. Rev. Lett. **119**, 237002 (2017).

[7] S. Hurand, A. Jouan, C. Feuillet-Palma, G. Singh, J. Biscaras, E. Lesne, N. Reyren, A. Barthélémy, M. Bibes, J. E. Villegas, C. Ulysse, X. Lafosse, M. Pannetier-Lecoeur, S. Caprara, M. Grilli, J. Lesueur, and N. Bergeal, Field-effect control of superconductivity and Rashba spin-orbit coupling in top-gated $LaAlO_3/SrTiO_3$ devices, Sci. Rep. **5**, 12751 (2015).

[8] D. A. Dikin, M. Mehta, C. W. Bark, C. M. Folkman, C. B. Eom, and V. Chandrasekhar, Coexistence of Superconductivity and Ferromagnetism in Two Dimensions, Phys. Rev. Lett. **107**, 056802 (2011).

[9] F. Bi, M. Huang, S. Ryu, H. Lee, C. W. Bark, C. B. Eom, P. Irvin, and J. Levy, Room temperature electronically controlled ferromagnetism at the $LaAlO_3/SrTiO_3$ interface, Nat. Commun. **5**, 5019 (2014).

[10] G. Cheng, M. Tomczyk, S. Lu, J. P. Veazey, M. Huang, P. Irvin, S. Ryu, H. Lee, C. B. Eom, C. S. Hellberg, and J. Levy, Electron pairing without superconductivity, Nature (London) **521**, 196 (2015).

[11] Ariando, X. Wang, G. Baskaran, Z. Q. Liu, J. Huijben, J. B. Yi, A. Annadi, A. Roy Barman, A. Rusydi, S. Dhar, Y. P. Feng, J. Ding, H. Hilgenkamp, and T. Venkatesan, Electronic phase separation at the $LaAlO_3/SrTiO_3$ interface, Nat. Commun. **2**, 188 (2011).

[12] A. F. Santander-Syro, O. Copie, T. Kondo, F. Fortuna, S. Pailhés, R. Weht, X. G. Qui, F. Bertran, A Nicolaou, A. Taleb-Ibrahimi, P. Le Févre, G. Herranz, M. Bibes, N. Reyren, Y. Apertet, P. Lecoueur, A. Barthélémy, and M. J. Rozenberg, Two-dimensional electron gas with universal subbands at the surface of $SrTiO_3$, Nature (London) **469**, 189 (2011).

[13] A. Joshua, S. Pecker, J. Ruhman, E. Altman, and S. Ilani, A universal critical density underlying the physics of electrons at the $LaAlO_3/SrTiO_3$ interface, Nat. Commun. **3**, 1129 (2012).

[14] T. C. Rödel, C. Bareille, F. Fortuna, C. Baumier, F. Bertran, P. Le Févre, M. Gabay, O. Hijano Cubelos, M. J. Rozenberg, T. Maroutian, P. Lecoeur, and A. F. Santander-Syro, Orientational tuning of the Fermi sea of confined electrons at the $SrTiO_3$ (110) and (111) surfaces, Phys. Rev. Appl. **1**, 051002 (2014).

[15] W. Siemons, G. Koster, H. Yamanoto, W. A. Harrison, G. Lucovsky, T. H. Geballe, D. H. A. Blank, and M. R. Beasley, Origin of Charge Density at $LaAlO_3$ on $SrTiO_3$ Heterointerfaces: Possibility of Intrinsic Doping, Phys. Rev. Lett. **98**, 196802 (2007).

[16] Z. Q. Liu, C. J. Li, W. M. Lü, X. H. Huang, Z. Huang, S. W. Zeng, X. P. Qiu, L. S. Huang, A. Annadi, J. S. Chen, J. M. D. Coey, T. Venkatesan, and Ariando, Origin of the Two-Dimensional Electron Gas at $LaAlO_3/SrTiO_3$ Interfaces: The Role of Oxygen Vacancies and Electronic Reconstruction, Phys. Rev. X **3**, 021010 (2013).

[17] S. K. Davis, Z. Huang, K. Han, Ariando, T. Venkatesan, and V. Chandrasekhar, Electrical transport anisotropy controlled by

oxygen vacancy concentration in (111) $LaAlO_3/SrTiO_3$ interface structures, Adv. Mater. Interfaces **4**, 1600830 (2017).

[18] C. W. Bark, D. A. Felker, Y. Wang, Y. Zhang, H. W. Jang, C. M. Folkman, J. W. Park, S. H. Baek, H. Zhou, D. D. Fong, X. Q. Pan, E. Y. Tsymbal, M. S. Rzchowski, and C. B. Eom, Tailoring a two-dimensional electron gas at the $LaAlO_3/SrTiO_3$ (001) interface by epitaxial strain, Proc. Natl. Acad. Sci. USA **108**, 4720 (2011).

[19] Z. Huang, K. Han, S. Zeng, M. Motapothula, A. Y. Borisevich, S. Ghosh, W. Lu, C. Li, W. Zhou, Z. Liu, M. Coey, T. Venkatesan, and Ariando, The effect of polar fluctuation and lattice mismatch on carrier mobility at oxide interfaces, Nano Lett. **16**, 2307 (2016).

[20] J. Hemberger, P. Lunkenheimer, R. Viana, R. Böhmer, and A. Loidl, Electric-field-dependent dielectric constant and nonlinear susceptibility in $SrTiO_3$, Phys. Rev. B **52**, 13159 (1995).

[21] Y. Han, S. Shen, J. You, H. Li, Z. Luo, C. Li, G. Qu, C. Xiong, R. Dou, L. He, D. Naugle, G. Guo, and J. Nie, Two-dimensional superconductivity at (110) $LaAlO_3/SrTiO_3$ interfaces, Appl. Phys. Lett. **105**, 192603 (2014).

[22] A. M. R. V. L. Monteiro, D. J. Groenendijk, I. Groen, J. de Bruijckere, R. Gaudenzi, H. S. J. van der Zant, and A. D. Caviglia, Two-dimensional superconductivity at the (111) $LaAlO_3/SrTiO_3$ interface, Phys. Rev. B **96**, 020504(R) (2017).

[23] M. M. Mehta, D. A. Dikin, C. W. Bark, S. Ryu, C. M. Folkman, C. B. Eom, and V. Chandrasekhar, Evidence for charge-vortex duality at the $LaAlO_3/SrTiO_3$ interface, Nat. Commun. **3**, 955 (2012).

[24] M. M. Mehta, D. A. Dikin, C. W. Bark, S. Ryu, C. M. Folkman, C. B. Eom, and V. Chandrasekhar, Magnetic field tuned superconductor-to-insulator transition at the $LaAlO_3/SrTiO_3$ interface journal, Phys. Rev. B **90**, 100506(R) (2014).

[25] S. K. Davis, Z. Huang, K. Han, Ariando, T. Venkatesan, and V. Chandrasekhar, Signatures of electronic nematicity in (111) $LaAlO_3/SrTiO_3$ interfaces, Phys. Rev. B **97**, 041408(R) (2018).

[26] L. Li, C. Richter, J. Mannhart, and R. C. Ashoori, Coexistence of magnetic order and two-dimensional superconductivity at $LaAlO_3/SrTiO_3$ interfaces, Nat. Phys. **7**, 762 (2011).

[27] J. A. Bert, B. Kalisky, C. Bell, M. Kim, Y. Hikita, H. Y. Hwang, and K. A. Moler, Direct imaging of the coexistence of ferromagnetism and superconductivity at the $LaAlO_3/SrTiO_3$ interface, Nat. Phys. **7**, 767 (2011).

[28] S. McKeown Walker, A. de la Torre, F. Y. Bruno, A. Tamai, T. K. Kim, M. Hoesch, M. Shi, M. S. Bahramy, P. D. C. King, and F. Baumberger, Control of a Two-Dimensional Electron Gas on $SrTiO_3$ by Atomic Oxygen, Phys. Rev. Lett. **113**, 177601 (2014).

[29] J. Ruhman, A. Joshua, S. Ilani, and E. Altman, Competition between Kondo screening and magnetism at the $LaAlO_3/SrTiO_3$ interface, Phys. Rev. B **90**, 125123 (2014).

[30] V. V. Bal, Z. Huang, K. Han, Ariando, T. Venkatesan, and V. Chandrasekhar, Electrostatic tuning of magnetism at the conducting (111) $(La_{0.3}Sr_{0.7})(Al_{0.65}Ta_{0.35})/SrTiO_3$ interface, Appl. Phys. Lett. **111**, 081604 (2017).

[31] S. Nandy, N. Mohanta, S. Acharya, and A. Taraphder, Effect of electron correlations on the Lifshitz transition at the $LaAlO_3/SrTiO_3$ interface, in *DAE Solid State Physics Symposium 2016*, edited by S. Bhattacharya, S. Singh, A. Das, and S. Basu, AIP Conf. Proc. No. 1832 (AIP, New York, 2017), p. 110026.

[32] D. Fuchs, A. Sleem, R. Schäfer, A. G. Zaitsev, M. Meffert, D. Gerthsen, R. Schneider, and H. v. Löhneysen, Incipient localization of charge carriers in the two-dimensional electron system in $LaAlO_3/SrTiO_3$ under hydrostatic pressure, Phys. Rev. B **92**, 155313 (2015).

[33] T. Hernandez, C. W. Bark, D. A. Felker, C. B. Eom, and M. S. Rzchowski, Localization of two-dimensional electron gas in $LaAlO_3/SrTiO_3$ heterostructures, Phys. Rev. B **85**, 161407(R) (2012).

[34] G. Herranz, F. Sánchez, N. Dix, M. Scigaj, and J. Fontcuberta, High mobility conduction at (110) and (111) $LaAlO_3/SrTiO_3$ interfaces, Sci. Rep. **2**, 758 (2012).

[35] S. Davis, V. Chandrasekhar, Z. Huang, K. Han, Ariando, and T. Venkatesan, Anisotropic multicarrier transport at the (111) $LaAlO_3/SrTiO_3$ interface, Phys. Rev. B **95**, 035127 (2017).

[36] P. K. Rout, I. Agireen, E. Maniv, M. Goldstein, and Y. Dagan, Six fold crystalline anisotropic magnetoresistance in the (111) $LaAlO_3/SrTiO_3$ oxide interface, Phys. Rev. B **95**, 241107(R) (2017).

[37] S. K. Davis, Z. Huang, K. Han, Ariando, T. Venkatesan, and V. Chandrasekhar, Superconductivity and frozen electronic states at the (111) $LaAlO_3/SrTiO_3$ interface, Phys. Rev. B **98**, 024504 (2018).

[38] S. K. Davis, Z. Huang, K. Han, Ariando, T. Venkatesan, and V. Chandrasekhar, Magnetoresistance in the superconducting state at the (111) $LaAlO_3/SrTiO_3$ interface, Phys. Rev. B **96**, 134502 (2017).

[39] D. Doennig, W. E. Pickett, and R. Pentcheva, Massive Symmetry Breaking in $LaAlO_3/SrTiO_3$ (111) Quantum Wells: A Three Orbital Strongly Correlated Generalization of Graphene, Phys. Rev. Lett. **111**, 126804 (2013).

[40] D. Xiao, W. Zhu, Y. Ran, N. Nagaosa, and S. Okamoto, Interface engineering of quantum Hall effects in digital transition metal oxide heterostructures, Nat. Commun. **2**, 596 (2011).

[41] V. V. Bal, Z. Huang, K. Han, Ariando, T. Venkatesan, and V. Chandrasekhar, Strong spin-orbit coupling and magnetism in (111) $(La_{0.3}Sr_{0.7})(Al_{0.65}Ta_{0.35})O_3/SrTiO_3$, Phys. Rev. B **98**, 085416 (2018).

[42] Z. Huang, N. Palina, S. W. Zeng, Z. Huang, C. J. Li, W. X. Zhou, D.-Y. Wan, L. C. Zhang, X. Chi, R. Guo, J. S. Chen, T. Venkatesan, A. Rusydi, and Ariando, Controlling Kondo-like scattering at the $SrTiO_3$-based interfaces, Sci. Rep. **6**, 25455 (2016).

[43] H. Z. Huang, S. W. Zeng, M. Yang, C. J. Li, W. X. Zhou, X. Renshaw Wang, T. Venkatesan, J. M. D. Coey, M. Goiran, W. Escoffier, and Ariando, Electrical properties and subband occupancy at the (La, Sr)(Al, Ta)$O_3/SrTiO_3$ interface, Phys. Rev. Mater. **1**, 011601(R) (2017).

[44] A. D. Caviglia, S. Gariglio, N. Reyren, D. Jaccard, T. Schneider, M. Gabay, S. Thiel, G. Hammerl, J. Mannhart, and J.-M. Triscone, Electric field control of the $LaAlO_3/SrTiO_3$ interface ground state, Nature (London) **456**, 624 (2008).

[45] M. Lee, J. R. Williams, S. Zhang, C. D. Frisbie, and D. Goldhaber-Gordon, Electrolyte Gate-Controlled Kondo Effect in $SrTiO_3$, Phys. Rev. Lett. **107**, 256601 (2011).

[46] P. Santhanam, Localization and superconductivity in thin films and narrow wires of aluminum, Ph.D. thesis, Northwestern University, 1985.

[47] A. Bergmann, M. Kaveh, and N. Wiser, Explanation of the anomalous T^4 behavior of the low-temperature electrical resistivity of silver, J. Phys. F: Met. Phys. **10**, L71 (1980).

[48] W. G. Baber, The contribution to the electrical resistance of metals from collisions between electrons, Proc. R. Soc. London Sect. A **158**, 383 (1937).

[49] X. Lin, B. Fauqué, and K. Behnia, Scalable T^2 resistivity in a small single-component Fermi surface, Science **349**, 945 (2015).

[50] J. H. Barrett, Dielectric constant in perovskite type crystals, Phys. Rev. **86**, 118 (1952).

[51] M. Ben Shalom, A. Ron, A. Palevski, and Y. Dagan, Shubnikov-De Haas Oscillations in $SrTiO_3/LaAlO_3$ Interface, Phys. Rev. Lett. **105**, 206401 (2010).

[52] M. M. Parish and P. B. Littlewood, Non-saturating magnetoresistance in heavily disordered semiconductors, Nature (London) **426**, 162 (2003).

[53] A. K. Nigam and A. K. Majumdar, Magnetoresistance in canonical spin-glasses, Phys. Rev. B **27**, 495 (1983).

[54] J. Inaba and T. Katsufuji, Large Magnetoresistance in spin and carrier doped $SrTiO_3$, Phys. Rev. B **72**, 052408 (2005).

[55] J. Eom, Electrical properties of mesoscopic spin-glasses, Ph.D. thesis, Northwestern University, 1998.

[56] P. W. Anderson, The absence of diffusion in certain random lattices, Phys. Rev **109**, 1492 (1958).

[57] P. A. Lee and T. V. Ramakrishnan, Rev. Mod. Phys. **57**, 287 (1985).

[58] B. Y. Jin, Y. H. Shen, H. Q. Yan, H. K. Wong, J. E. Hilliard, and J. B. Ketterson, Transport properties in weak and strong localization regime of $Nb_{0.53}Ti_{0.47}/Ge$ superlattices Superlattices Microstruct. **1**, 401 (1985).

[59] A. Punnoose, Magnetoconductivity in the presence of Bychkov-Rashba spin-orbit interaction, Appl. Phys. Lett. **88**, 252113 (2006).

[60] Y. Kim, R. M. Lutchyn, and B. Nayak, Origin and transport signatures of spin-orbit interactions in one- and two-dimensional $SrTiO_3$-based heterostructures, Phys. Rev. B **87**, 245121 (2013).

[61] D. Rainer and G. Bergmann, Multiband effects in weak localization, Phys. Rev. B **32**, 3522 (1985).

[62] S. Maekawa, and H. Fukuyama, Magnetoresistance in two-dimensional disordered systems: Effects of Zeeman splitting and spin-orbit scattering, J. Phys. Soc. Jpn. **50**, 2516 (1981).

[63] S. Hikami, A. Y. Larkin, and Y. Nagaoka, Spin-orbit interaction and magnetoresistance in the two-dimensional random system, Prog. Theor. Phys. **63**, 707 (1980).

[64] G. Bergmann, Weak localization in thin films: A time-of-flight experiment with conduction electrons, Phys. Rep. **107**, 1 (1984).

[65] B. L. Al'tshuler, A. G. Aronov, A. I. Larkin, and D. E. Khmelnitskiĭ, Anomalous magnetoresistance of semiconductors, Zh. Eksp. Teor. Fiz. **81**, 768 (1981) [Sov. Phys. JETP **54**, 411 (1982)].

[66] A. Houghton, J. R. Senna, and S. C. Ying, Diffusion of electrons in two dimensions in arbitrarily strong magnetic fields, Phys. Rev. B **25**, 2196 (1982).

[67] L. G. Aslamazov and A. I. Larkin, The influence of fluctuation pairing of electrons on the conductivity of normal metal, Phys. Lett. A **26**, 238 (1968).

[68] K. Maki, Critical fluctuation of the order parameter in type-II superconductors, Prog. Theor. Phys. **39**, 897 (1968).

[69] W. J. Skocpol and M. Tinkham, Fluctuations near superconducting phase transitions, Rep. Prog. Phys. **38**, 1049 (1975).

[70] Z. Zhong, A. Toth, and K. Held, Theory of spin-orbit coupling at $LaAlO_3/SrTiO_3$ interfaces and $SrTiO_3$ surfaces, Phys. Rev. B **87**, 161102(R) (2013).

[71] J. Biscaras, S. Hurand, C. Feuillet-Palma, A. Rastogi, R. C. Budhani, N. Reyren, E. Lesne, J. Lesueur, and N. Bergeal, Limit of the electrostatic doping in two-dimensional electron gases of $LaXO_3$(X = Al, Ti)/$SrTiO_3$, Sci. Rep. **4**, 6788 (2014).